
Article:
Mustafa, BG, Kiah, MHM, Irshad, A et al. (4 more authors) (2019) Rich biomass combustion: Gaseous and particle number emissions. Fuel, 248. pp. 221-231. ISSN 0016-2361

https://doi.org/10.1016/j.fuel.2019.03.027

Fuel **248**:221-231 15 Jul 2019 https://doi.org/10.1016/j.fuel.2019.03.027

Rich Biomass Combustion: Gaseous and Particle Number Emissions

Bintu G. Mustafa[a,b*], Miss H. Mat Kiah[a,c], Aysha Irshad[a,d], Gordon E. Andrews[a], Herodotos N. Phylaktou[a], Hu Li[a] and Bernard M. Gibbs[a]

[a] School of Chemical and Process Engineering, University of Leeds, Leeds, LS2 9JT, UK
[b] Chemical Engineering, University of Maiduguri, Bama Road, P.M.B 1069, Maiduguri, Nigeria.
[c] Energy Engineering Department, Faculty of Chemical and Energy Engineering, Universiti Teknologi, Malaysia (UTM), 81310 Skudai, Johor, Malaysia
[d] Dept. of Chemical Engineering, University of Engineering & Technology, Lahore, Pakistan

ABSTRACT

The cone calorimeter is a standard test method for material behaviour in fires. The principle of the cone calorimeter is to use an electric radiant heater to raise the temperature of the combustion zone and ignite the fuel and 35 kW/m^2 was used in the present work, as this has been previously shown to be sufficient to establish fully developed combustion of biomass materials such as wood. As one of the main fire loads is wood and wood is the dominant biomass for energy generation, it is reasonable to use the cone calorimeter to characterize the combustion of biomass on a small scale and pine was used in the present work. The cone calorimeter was used in the controlled atmosphere mode with an enclosure around the test biomass that enabled the air flow for biomass combustion to be controlled at 19.2 g/m^{2}s, which corresponds to a combustion heat release rate HRR of 57 kW/m^2, assuming all the oxygen in the air is consumed. This air flow will be shown to generate rich combustion at a metered equivalence ratio, Ø, of about 2, which is comparable with the first gasification stage of biomass two stage burning in log burners and pellet burners, where air is added downstream of the gasification stage of biomass combustion. Soot emissions are generated in this rich gasification stage burning and potentially oxidized in the oxidation second stage burning. The rich burning gasification zone particulate emissions were analysed for number size distribution using the Cambustion DMS 500 particle size analyser. The exit from the controlled combustion zone was extended in a 75 mm diameter chimney where a mean gas sample was taken. A heated Gasmet FTIR was used for gas composition analysis, using a heated sample line, filter and pump from the sample point to the analyser. The particles emitted were sampled after the second stage combustion from entrained air into the chimney discharge gases into a dilution tunnel with a fixed gas flow rate of 24 l/s, which gave a

* Corresponding Author. Tel: +447741382667
E-mail address: pm08bgm@leeds.ac.uk, bintgrem@yahoo.co.uk (Bintu Grema Mustafa)

Fuel **248**:221-231 15 Jul 2019 https://doi.org/10.1016/j.fuel.2019.03.027

dilution ratio of the primary combustion gases of 150/1 which is required for nano-particle size analysis. A Cambustion DMS500 electrical mobility particle number and size instrument was used with size resolution from 5 to 1000 nm. The present results show that in the rich burning first stage chimney sample there were very high levels of 20 nm nanoparticles, 1 x 10^{10}/cc, and an accumulation mode peak at 200 nm. The presence of the 20 nm particles makes the particulate emissions extremely toxic.

Keywords: biomass combustion, FTIR, particle size, gaseous emissions.

1 INTRODUCTION

In the mid-1990s, epidemiological data in the USA and UK showed that 1% extra deaths occurred for every 10 µg/m^3 of PM_{10} in ambient air within days of the high particulates [1-3]. Epidemiologic studies have linked fine particulates in air pollution with cardiopulmonary mortality [2]. The only medical explanation of this effect is that particles <50 nm must be present [4] as they cause alveolar inflammation and blood thickening [5], which reduces lung function and places a strain on the heart. This epidemiological data is based on correlations of PM_{10} in the atmosphere and hospital admissions and asthma drug demand. The medical explanation [4] involves the presence of solid nano-particles in the alveolar region of the lungs and the composition of these particles is not significant [4]. However, other evidence of health effects of fine particles include allergic reactions, chronic obstruction pulmonary disease (COPD), pulmonary fibrosis and lung cancer [6], indicate that the chemicals absorbed on the particles may also be part of the health effects of ultra-fine particles.

Altaher et al. [7] have shown that for biomass pellet heaters particulate mass emissions, the filter paper based particle mass emissions were in the range 23 – 85 mg/m^3. Linda and Johansson [8] surveyed a range of biomass combustion equipment and reported PM emissions for pellet burners from 62 – 180 mg/m^3. However, they did show that older biomass combustion systems were much worse for PM emissions. In wood fires, in ventilation-controlled compartment fires the particle production is about 100 mg/m^3 [9], which is similar to that found in biomass burners. A person breathes about 10 m^3 of air per day which at 10 µg/m^3 is a lung loading of 0.1 mg. Breathing biomass smoke directly at 100

mg/m^3 would give the 0.1 mg lung loading in 86 s. Even with dilution of biomass smoke by a factor of 10,000 in the atmosphere, the concentration would be 10 µg/m^3, so that clearly biomass particulate mass emissions are a health problem [6].

Altaher et al. [7] showed that the particle emissions from biomass pellet combustion had a particle size distribution in the nano-particle range with a peak number at 30nm of 5 x 10^8/cc. Migliavacci et al. [10] found a peak number of 1.55 x 10^8/cm^3 at 150 nm. Nussbaumer and Lauber [11] also found a peak number size of 160 nm but had a lower number of 8 x 10^7. Bologa et al. [12] found a peak particle number of 5 x 10^7/cm^3 at 60 nm. Michel et al. [13] determined the particle size distribution for a 50 kW pellet boiler for pellets made from poplar wood. Their results show that the particle size where the peak number of particles occur was 65 nm for the raw pellets and the peak number of particles was 3.1 – 3.7 x 10^8/cc. This evidence shows that particles from biomass combustion are in the size range that gives a health problem with mass emissions that are also significant. Despite the health hazards associated with biomass particulate emissions, very few investigations have been done on ultra-fine particulate emissions from biomass combustion. In the present work using rich combustion (gasification conditions) results in ultra-fine particle emissions with higher numbers than in the above works were obtained.

Particle sizes are generally of the order of 1 µm from spherical droplets of smouldering fires while those of irregular soot particulates found at the stage of flaming combustion appear larger and difficult to determine and basically depend on the measuring technique and sampling position [14]. Hertzberg et al. [15] used the controlled atmosphere cone calorimeter to determine the particle sizes of carbon in wood fires, but did not investigate the under ventilated conditions which generate the rich combustion that leads to the rapid carbon formation demonstrated in the present work.

2 MATERIALS AND METHODS

2.1 The Fuel Properties

Construction pine wood was the biomass used in the present work, with the fuel characteristics shown in Table 1. A Parr 6200 oxygen bomb calorimeter was used to determine the gross calorific value of the pine. The Ultimate Analysis in Table 1 was carried out using the Thermo Flash EA 2000 Elemental Analyser to determine the CHONS compounds in the pine wood. The proximate analysis in Table 1 used thermal gravimetric analysis, the Shimadzu TGA-50 with a TA60WS processor, to determine the water, volatiles, fixed carbon and ash content. The TGA analysis of the volatile (excluding water) is shown in Fig. 1 as normalised volatile mass loss as a function of temperature. The present pine biomass is shown to be typical of a wide range of other biomass in terms of the temperature at which volatiles are released.

Table 1: Fuel Properties

Parameter	Pine Wood Sticks
Proximate Analysis (Wt. %) (daf)	
Volatile Matter	86.54%
Fixed Carbon	13.46%
Ultimate Analysis (Wt. %) (daf)	
Carbon	53.95%
Hydrogen	6.79%
Nitrogen	0.11%
Sulphur	0.0%
Oxygen	39.15%
Stoichiometric (Air to Fuel Ratio) A/F by carbon balance	5.89
Gross Calorific value	18.9 MJ/kg
Moisture (as received)	6.18%
Ash (as received)	2.27%

2.2 The Controlled Atmosphere Cone Calorimeter

The controlled atmosphere cone calorimeter that was used is shown in Fig. 2 and is a modification of the standard cone calorimeter detailed in ISO 5660 [16], to create a rich combustion (oxygen reduced

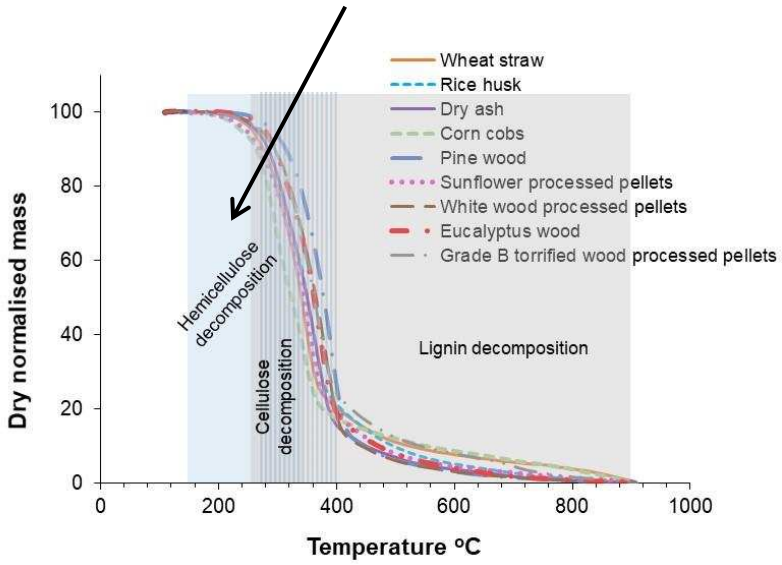

Fig. 1. Normalised volatile mass loss as a function of temperature for pine wood and a range of other biomass.

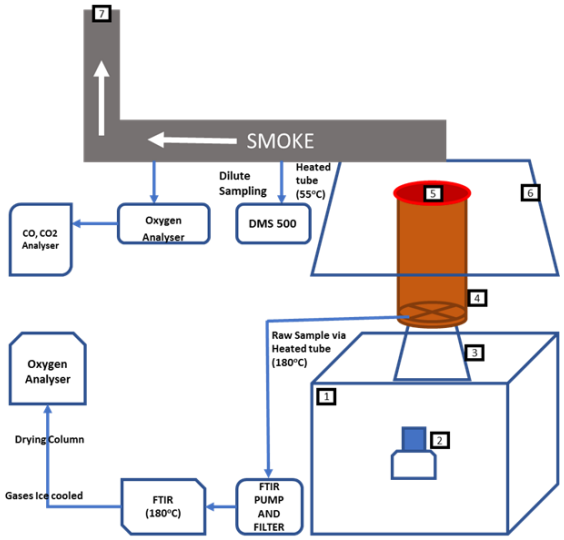

1. The Controlled Atmosphere Compartment
2. Load cell and specimen holder
3. The cone heater
4. The chimney
5. The orifice plate
6. The hood
7. Gases exit for safe disposal

Fig. 2. Controlled Atmosphere Cone Calorimeter

environment). The introduction of the enclosure makes the controlled atmosphere cone calorimeter capable of creating the combustion conditions of gasified stage 1 combustion of a two staged biomass

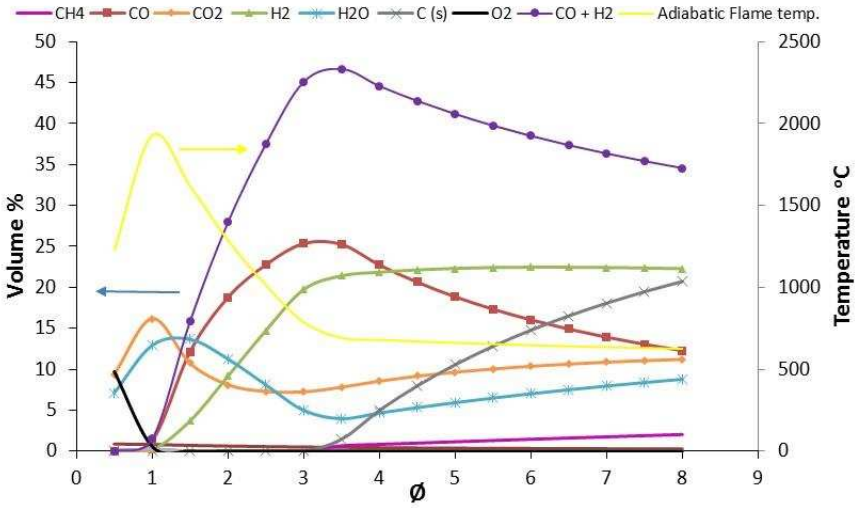

Fig. 3. Equilibrium concentrations and adiabatic flame temperature of gaseous products as a function of equivalence ratio (Ø) for pine wood gasification using CEA software.

burner. The CEA (Chemical Equilibrium and Applications) software by NASA was used to perform the thermodynamic equilibrium calculations of the gasification of biomass to predict the composition of gases as a function of equivalence ratio Ø. Equilibrium computations for the products of combustion of pine wood of the composition in Table 1 is shown in Fig. 3. This shows that the peak CO and H_2 composition of the gaseous products of adiabatic equilibrium combustion of pine occurs at Ø=3. There are no equilibrium hydrocarbons, apart from very low levels of methane. It will be shown in the results that the rich non-adiabatic combustion of pine has considerable hydrocarbon content indicating that the test conditions are not adiabatic due to heat losses from the combustion zone. As a result, measured CO are lower than in Fig. 3.

The cone calorimeter was operated with a controlled air supply design to create rich combustion conditions that occur in air starved compartment fires. The steel box enclosed the balance/sample holder and the cone heater and had a metered air supply through the two access ports in the bottom of the air tight box. The airtight box was 38 cm long, 30 cm wide and 33 cm high, a volume of 0.0376 m^3. In developing this experimental method, it was found that the metal box had excessive heat losses that influenced the temperature of the test specimen and hence influenced the heat release rate, HRR. To improve the design the airtight box was insulated from the inside and the door from the outside using an insulation board to avoid heat loss as a result of heating the stainless steel. The cone

calorimeter enclosure also had a glass window for the observation of the combustion and this was insulated when not being used for viewing the flame. The test specimen was also insulated underneath to prevent heat losses to the supporting metal cylinder leading to the load cell, this also protected the load cell from overheating.

The airflow to the combustion chamber was measured using a variable air flow meter and the air flow could be varied from 6 – 28 l/min from a compressed air supply, which is 0.12 – 0.56 g/s air mass flow. This is a range of about 10 – 50 air changes per hour (ACH), but although this is useful in terms of compartment ventilation it is rather arbitrary in the present work as the volume of the enclosure could in principle be any size. A more fundamental parameter is considered to be the air mass flow per exposed surface area of the test specimen (0.01 m^2). The air flow range in these terms is 12 – 56 g/sm^2. Another way of looking at the ventilation conditions is to use the fact that for all HCON fuels there are 3.05 MJ of heat release per kg of air and this converts the air mass flow range into fire HRR in kW as 0.37 – 1.71 kW fires and in terms of the exposed surface area of the wood is 37 – 171 kW/m^2. In the present work a single air flow was used of 19 g/sm^2 or 58 kW/m^2, as the aim was to demonstrate that the equipment could be used to investigate biomass combustion characteristics in a controlled burning zone equivalence ratio, Ø.

The air flow to the combustion zone dominated the gas mass flow in the exhaust chimney, which without combustion was 0.19 g/s. The cone calorimeter total gas flow was controlled at 24 l/s, measured by a standard orifice plate flow meter. This, at ambient conditions, is a mass flow of 28.8 g/s. This is an air dilution of the gasification zone flow of 150.6/1. With combustion the products of combustion add to the compartment chimney discharge flow and this decreases the dilution ratio slightly. It will be shown that the operating equivalence ratio at the above test conditions was about 2 and this gives for pine an A/F of 2.95/1. This increases the exhaust mass flow to 0.254 g/s, which gives a dilution ratio of 146/1. Sampling for particle number analysis using the Cambustion DMS500 particle size analyser has to be undertaken in diluted flow and as the cone calorimeter dilutes the products of the initial combustion zone, to prevent water condensation, the diluted sample is ideal for

particle size analysis and was used in the present work. The measured particle number was corrected using the above dilution ratio to determine the concentration of particles in the chimney. This assumes that there was no post oxidation of particles, which is a reasonable assumption as carbon does not burn in air below 600^{o}C and the chimney temperature was well below this.

The entrainment of ambient air downstream of the chimney can give oxidation of the volatile gases from the rich combustion zone and this represents the second stage combustion of two stage biomass burners. This second stage burning was not the main purpose of the present work, which concentrated on the rich first stage gasification combustion. However, oxygen consumption calorimetry [17] was used to determine the overall heat release from a paramagnetic oxygen analysis of the diluted gases in the cone calorimeter. In addition, the rich zone heat release was determined by paramagnetic oxygen analysis of the chimney raw gas analysis at the exit from the heated FTIR, after separation of the water in an ice trap. The water content of the hot sample gases was determined by the FTIR and this was used to correct the dry oxygen analysis to a wet based analysis. This enabled the primary and overall heat release to be determined and by difference the heat release in the second stage air addition could be determined. In this work these two heat release stages will be referred to as the primary and overall heat release, with the dilution stage post fire heat release referred to as the secondary heat release zone.

2.3 Experimental Procedures

The conical radiant heater in the cone calorimeter is used for two purposes: firstly, to determine the minimum radiant ignition energy of the test material; and secondly, to enable combustion of a small test specimen of material to be undertaken in the presence of radiation from a larger combustion zone and it is this use of the cone calorimeter that is most important in the present work. Obviously, the choice of the radiant heat intensity is significant and higher radiant heat essentially simulates a hotter fire. In the present work the pine wood was exposed to the conical heater of the cone calorimeter radiating at 35 kw/m^2 with a constant air mass flow for each test. This is the recommended standard heat flux recommended by British Standards [16] for use in material evaluation for performance in

fires using the standard cone calorimeter [16]. Also, 35 kW/m^2 was recommended by Flecknoe-Brown et al. [18]. Herzberg and Blomqvist, [15] noted that 35 kW/m^2 was a "trade-off between a lower value, which possibly would have caused materials to pyrolyse only, and a higher value which might have provoked an unrealistically clean burning behaviour".

Five 100 x 20 x 20 mm (L x W x H) rectangular shaped pine sticks were arranged in the 100 x 100mm square sample holder of the cone calorimeter and tested in a horizontal orientation with the top surface exposed to the applied radiant heat flux. The initial weight of the wood was determined by the load cell as 128 g. The load cell was checked with reference weights at the start of each test programme and was very stable. The 35 kW/m^2 radiant heat flux caused the thermal decomposition of the samples leading to autoignition of the evolved gases and the autoignition delay time was determined in the tests at 29 s, so it was a very small part of the much longer burn time. The fire continued until flaming combustion ceased and there was only char burning. It will be shown that this transition from flaming combustion to char smouldering combustion was associated with a significant change in the particle size distribution.

2.4 The Gas Sampling System

The controlled atmosphere cone calorimeter was modified to enable a raw gas sample to be obtained from the exit from the chamber. A 40-hole X sample probe was mounted on top of the exit plane of the cone heater for the sampling of the mean composition of the raw gases. The X probe was mounted in a 76 mm diameter duct with flanges to join the cone heater exit to the chimney. This gas sample probe duct was 40 mm long. An 80 mm diameter chimney, the same diameter as the cone outlet, and 210 mm long was mounted on top of the sample probe in the 76 mm internal diameter tube and the total chimney length was 250 mm. It was found that when the fire was rich burning at low air flow rates, oxygen was detected in the sample probe, which should not occur. It was concluded that air was back flowing down the chimney. Part of the problem was the 3 lpm sample flow rate of the gas analyser that was significant relative to the air flow to the test section. To stop this air backflow, a grid plate was placed at the chimney exit to increase the exhaust flow pressure loss which then prevented

back flow of air down to the sample probe. This orifice plate on the chimney had five 6.3 mm diameter holes.

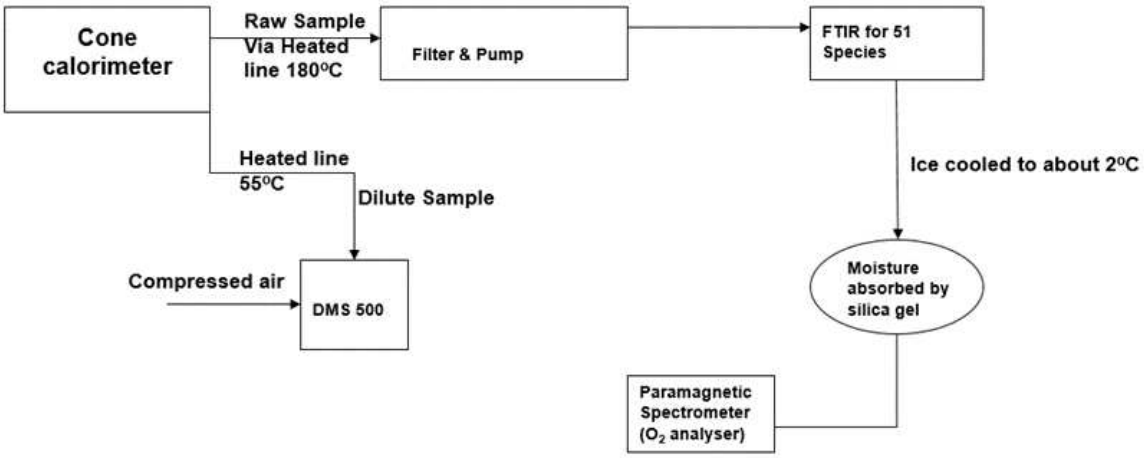

Fig. 4. Schematic of the gas analysis heated sample flow system

The sample gas transport system to the gas analysers is shown schematically in Fig. 4. A heated 180°C sample line was used to transport the gases from the exhaust to a 180°C heated pump (3 lpm) and filter and then there was another heated line to transport the gases to the 180°C heated Gasmet FTIR. The raw gas sample prevented any post oxidation of species by dilution of the gases with ambient air, as the gases were entrained into the cone calorimeter diluted flow metering section. Also, it prevented any losses of condensable gases that would occur if the exhaust was simply thermally cooled [19]. The gas sample from the FTIR outlet was transported via a PTFE tube to a refrigeration cooler of about 2°C and a silica gel column for the removal of water vapour before entering a paramagnetic oxygen analyser and then was discharged through the cone calorimeter discharge duct.

For particle size analysis a diluted sample is required for two reasons. Firstly, the dilution lowers the dew point by cooling and reducing the concentration and this prevents water vapour from the combustion products appearing as droplets and being counted as particles. However, higher molecular weight unburned hydrocarbons from the fire can form liquid aerosols in the dilution process and these are part of the particles that may be a health hazard. The cancer forming PAH fraction of hydrocarbons are likely to be generated as liquid aerosols from wood combustion [20]. If the fire forms acidic gases then with the water vapour present acid droplets can form, for example acetic acid droplets may be

possible in the present work. In the present work it is not known whether particles in any size range are liquid or solid or a mixture of both. Andrews et al. [9] have used gravimetric filter papers to determine the particle mass in fires and they showed that for pine wood fires the particle mass was 80% volatile. Thus, a high proportion of liquid aerosol particle emissions are anticipated in the present work on particles from fires. Particles are defined in other areas, such as diesel emissions as anything that is collected on a defined filter paper from an exhaust cooled by dilution to below 47ºC +/- 5ºC. This temperature is set to avoid condensing water on the filter paper. Andrews et al. [9] collected the particulates from fires with the filter paper heated to 47ºC but used thermal cooling rather than dilution cooling. This is acceptable for mass particulate collection but not for number measurement due to thermophoretic particle losses to the cooled wall.

The second reason for particle number size distribution needing to be measured in a diluted sample is that for low dilution particles agglomerate in the sampling system and the size distribution changes and the number of particles is reduced. Usually a dilution ratio of around 100/1 or more is advocated [21, 22]. The cone calorimeter dilutes the products of combustion from the cone heater outlet (chimney outlet in the present case) with ambient air. Thus, a diluted gas sample for particle size analysis taken from the cone calorimeter dilution tunnel is the obvious choice of gas sample location. The sample point was close to where the smoke production was measured in the cone calorimeter using the standard obscuration meter, so that particle number and smoke obscuration can be directly compared. It was shown above that at the present test conditions the dilution ratio was 146/1 and hence meets Kittelson's [22] recommended dilution ratio of >100/1.

The sample for particle number analysis was taken from the cone calorimeter dilution tunnel via a 55ºC heated line to the Cambustion DMS500 particle size analyser [23]. The dilution of fire products in the cone calorimeter from the chimney used ambient laboratory air. A problem in using ambient air for dilution in the cone calorimeter is that this air also has ultra-fine particles in it and for low particle number concentrations the dilution air would be HEPA filtered. However, it will be shown that the particulate numbers were orders of magnitude higher than for diesel engines and hence the error from

particles in the dilution air would not be significant. The 55ºC heated line was to allow dilution of the sample gas which serves to lower the dew point of the air so that condensation does not take place in the instrument. The DMS500 particle size analyser has an internal 10/1 diluter and the particle concentration provided by the instrument includes this dilution.

2.5 Toxic Gas Measurement using the Gasmet FTIR

The Gasmet heated FTIR gas analyser was calibrated by the manufacturers for over 60 gaseous species of importance in biomass combustion and has been used by the authors for research on fire toxicity for many years [9, 24-28]. The FTIR was zeroed on nitrogen each day, but no further calibration was necessary. The Gasmet FTIR is fully heated in the measurement section and this enables gases from the fire to be transported via the heated samples lines and pumps shown in Fig.4, with no oxidation or condensation losses occurring. Heated FTIR is the essential instrument for fire gas toxicity measurements and the Gasmet FTIR has an Environment Agency MCerts approval for legislated flue gas measurements.

2.6 Particle Measurement Equipment (DMS 500)

The Cambustion DMS 500 (Differential Mobility Spectrometer) [23] particle size measurement equipment was used to measure real time particle sizes in the size range 5 – 1000 nm. The DMS 500 size separates particles based on their electrical mobility and the size may be different from an aerodynamic mobility analyser. Electrical mobility is the dominant mode of particle size measurement for nano-particles. The DMS 500 responds to both liquid aerosols, which may occur in the present work from the volatile release from wood, and solid aerosols of soot and ash particles. It is a transient instrument and can take several size distributions per second. In the present work the size distribution as a function of the fire time duration was measured.

The particle number p/cm^3 size distribution was converted into a mass size distribution, g/m^3, by assuming the particles were spherical in shape with a density of 1000 kg/m^3. There are two common assumptions in this conversion, both of which are not valid. The nanoparticles (<50 nm) are generally

spherical, but the agglomeration mode particles (50-1000 nm) will form complex clusters of particles, having larger overall size and a non-spherical shape. The density of 1000 g/m^3 is a common assumed density for carbon and yet the particles are not all carbon. For diesel particulate emissions Andrews et al. [29] used gravimetric measurements with aerodynamic size separation to determine the effective density of particles as a function of size, using the assumption that the particles were spherical. Similar work is required for particulate emissions from fires, but for this work the common assumption of spherical particles of constant density will be used.

2.7 Heat Release Rate Calculations

The overall heat release rate HRR was calculated using the standard oxygen consumption calorimetry of the cone calorimeter methodology [17, 30]. Oxygen consumption calorimetry is based on the stoichiometric A/F ratio and calorific value which shows that for all fuels there is 3.05 MJ/kg$_{air}$ heat release per mass of air consumed, which is 13.1 MJ/kg$_{oxygen}$ [17, 30]. The cone calorimeter measures the oxygen in the diluted gases and from this and the measured mass flow rate of diluted gases the cone calorimeter calculates the HRR. The HRR may also be calculated from the measured fire load mass loss rate times the calorific value, this is less reliable as it assumes that all the mass lost is burned and consumes oxygen. However, in the air starved fires investigated in the present work combustion is incomplete and the HRR needs correcting for the combustion efficiency. The primary HRR in the present work are from the oxygen mass consumption method using the oxygen measured in the chimney gas sample. This is measured on a dry gas basis after extraction of water by cooling the gas sample in an ice cooler. The oxygen concentration has then to be converted to a wet gas basis and the water measurement by the FTIR is used for this correction. The oxygen mass concentration is then combined with the chimney mass flow rate (air inlet plus fuel mass loss rate) to give the mass flow of oxygen in the chimney, which enables the oxygen mass consumption and HRR to be determined as the inlet oxygen mass flow is known from the metered air inlet flow. The difference of the primary HRR from the overall HRR gives the secondary HRR in the discharge from the chimney as the air is entrained into the hot gases and combustion of CO and unburnt hydrocarbons is completed.

Fuel **248**:221-231 15 Jul 2019 https://doi.org/10.1016/j.fuel.2019.03.027

3 RESULTS AND DISCUSSION

3.1 Mass Loss Rate

The mass loss of the pine wood during the fire is shown in Fig. 5 as a function of time. The result shows a near constant mass loss rate from 200 – 1000 s. There was then from 1000 to 1200 s an increased mass loss rate. Finally, there was a reduced mass loss rate from 1200 to 1900 s, with the visible flame going out in the middle of this period, as marked on Fig. 5. After the flame went out the char was burning as smouldering combustion at a low mass loss rate.

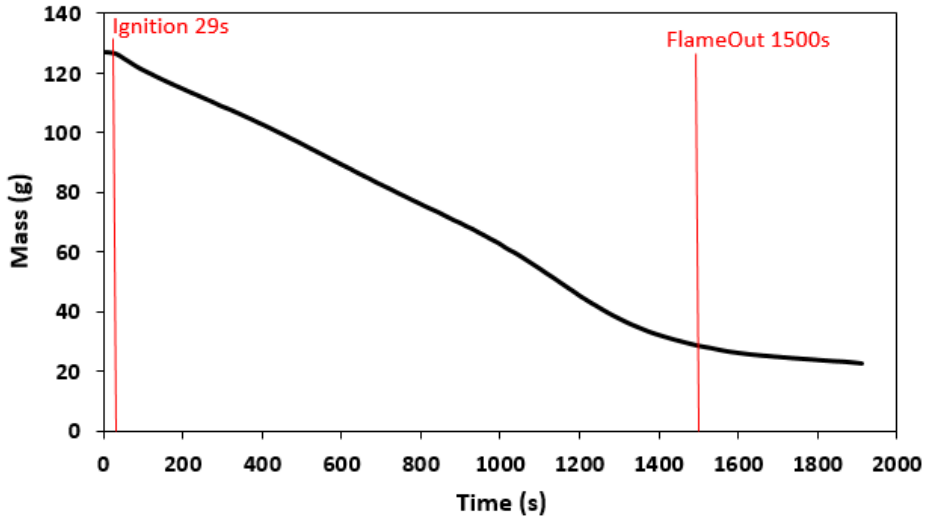

Fig. 5. Mass loss as a function of time

From 200 to 1000 s the mass loss rate was roughly constant at about 0.07 g/s. If the gross calorific value GCV of the raw wood is used at 18.9 MJ/kg then this is a steady state HRR of 1.32 kW or 132 kW/m^2. It will be shown below that this is higher than the primary oxygen consumption HRR due to the combustion inefficiency of rich combustion. The high CO and hydrocarbons from the rich fire complete combustion as air is entrained into the discharge jet from the chimney. The secondary HRR is determined from the difference in the overall HRR and the primary HRR and is shown to be significant.

Fig. 5 shows that the char phase of combustion was relatively slow and at the end of the recorded period the char was 20 % of the initial mass. This is higher than the 15.7 sum of fixed carbon and ash in the pine wood in Table 1 and this indicates that it is not just carbon and will also contain some HCO compounds of higher molecular weight MW and high boiling point. However, char has a higher

calorific value CV than for the initial wood and thus the energy content of the char is a greater proportion of the initial energy. Taking the char as carbon with a GCV as 32.8 MJ/kg with the GCV of the pine wood as 18.9 MJ/kg, the energy in 20 % of the char at the end of the test was 34.7 % of the total pine energy. This reduces the GCV of the gases burnt in the flaming combustion phase to 12.3 MJ/kg on average or 64.3 less than the GCV for all the wood burning. This has been shown in related work of the authors to agree with the measurements of all the energy content of the gases produced by the heating of wood in nitrogen on the same equipment as in the present work. The total mass flow of gases in the chimney flow agreed with the rate of mass loss of the wood and this indicates that all the major species in the gas had been identified by the FTIR. Hydrogen is a product of rich combustion, as shown in Fig. 3, and this is not measured by the FTIR. Hydrogen was calculated from the measured CO using the water gas shift reaction [19].

3.2 Heat Release Rate

The oxygen consumption overall or total heat releases rate (HRR) results are shown as a function of time in Fig. 6, together with the primary HRR by oxygen consumption and the HRR derived from the mass loss rate times the GCV of pine. The ignition delay at a radiant heating of 35 kW/m^2 was 29 s. At a heat flux of 35 kW/m^2 the total HRR was about 50 kW/m^2 throughout the flaming combustion phase from 200 to 1000 s. The difference between the total and primary HRR was very small and was only significant between 1000 s and 1500 s just before flameout. This small difference shows that there was little secondary combustion as the entrained cold air cooled the discharge from the chimney and stopped CO and HC oxidation.

The HRR by mass loss rate was about 130 kW/m^2. The reason for this difference, from the lower values in Fig. 6 for the primary HRR by oxygen consumption, is that the aim of the primary zone is to burn the fuel rich and pass rich product gases to the secondary zone. The difference is the potential HRR in a properly designed second stage burner.

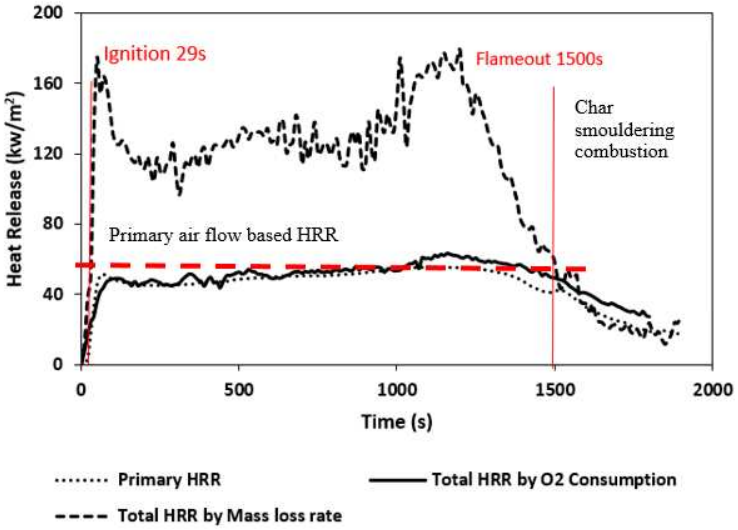

Fig. 6. Primary and Overall Heat Release Rates

These results do show that HRR in solid material fires should not be determined from the mass loss rate and the GCV for the original solid material. This is why the cone calorimeter oxygen consumption HRR measurement method was developed. The primary HRR is equal to the theoretical HRR of 58 kW/m^2 for 1100 – 1300 s, based on the constant air flow to the ventilation-controlled fire compartment. The lower values are due to the combustion efficiency and this is represented by increases in oxygen in the periods where hydrocarbons are high as shown in Fig. 7.

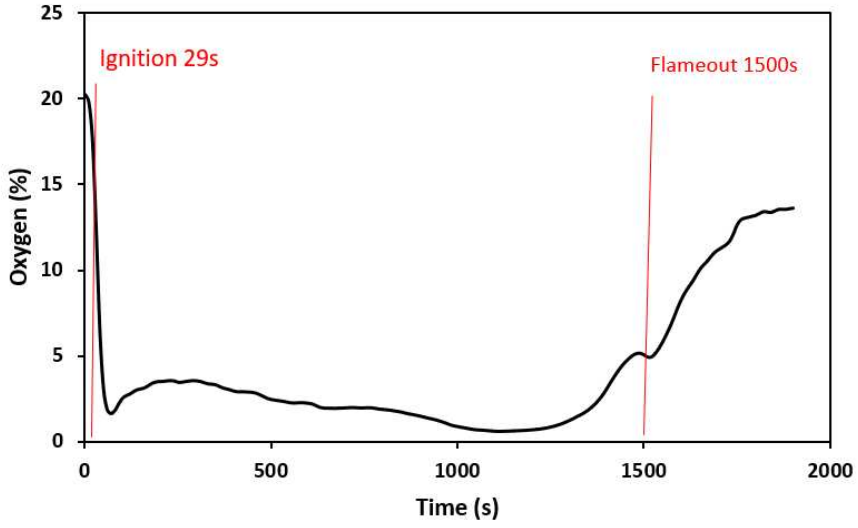

Fig. 7. Oxygen as a function of time for confined burning of pine

3.3 Equivalence Ratio

The fire equivalence ratio in the ventilation-controlled compartment is shown in Fig. 8 as a function of time. This is the equivalence ratio based on the ratio of the stoichiometric A/F by mass to that of the measured A/F mass ratio of the metered air flow and the mass loss rate of wood in the fire. This shows that the combustion was rich, or ventilation controlled throughout the flaming combustion phase, but was lean or fuel controlled in the char burning phase. Fig. 8 shows that there were two periods with mixtures richer than the mean and this was the first phase of flaming combustion up to 200 s and the 1000 – 1250 s period towards the last phase. It is possible that this last phase of rich combustion was due to oxidation of char. Fig. 8 also shows the measured mass loss rate and as the air flow was held constant the variation in equivalence ratio was due to the variation in the rate of fuel mass loss.

The assumption inherently made in Fig. 8 is that there is a constant stoichiometric A/F through the combustion time. This is not valid as the composition of the gases and solids that were burning varied with time through the fire. The combustion of mainly carbon in the smouldering combustion phase had a stoichiometric A/F of 11.4/1 instead of ~6/1 for the wood. However, it is the convention in fire research to treat the fuel as a fixed composition throughout the fire, so that the fire equivalence ratio in Fig. 8 should be comparable with any other fire equivalence ratio in the literature. The key feature is that the flaming combustion is very rich, as it is in ventilation-controlled compartment fires [24-28].

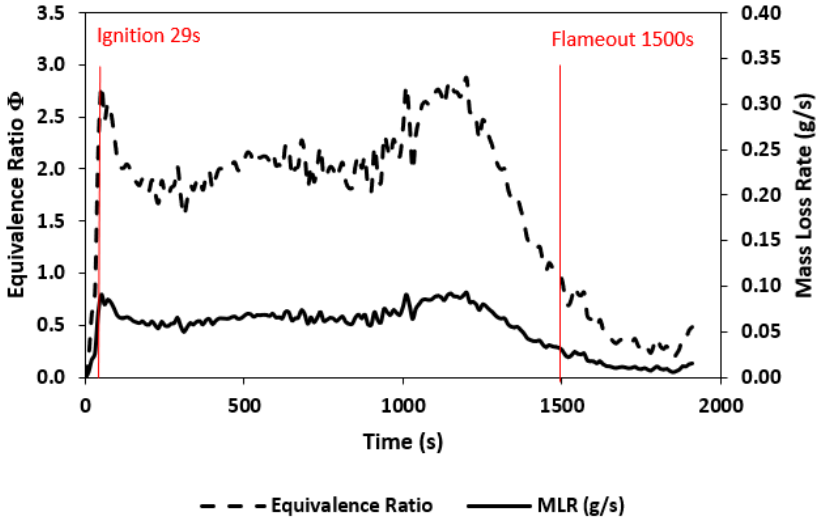

Fig. 8. Fire wood mass consumption rate and metered equivalence ratio as a function of time.

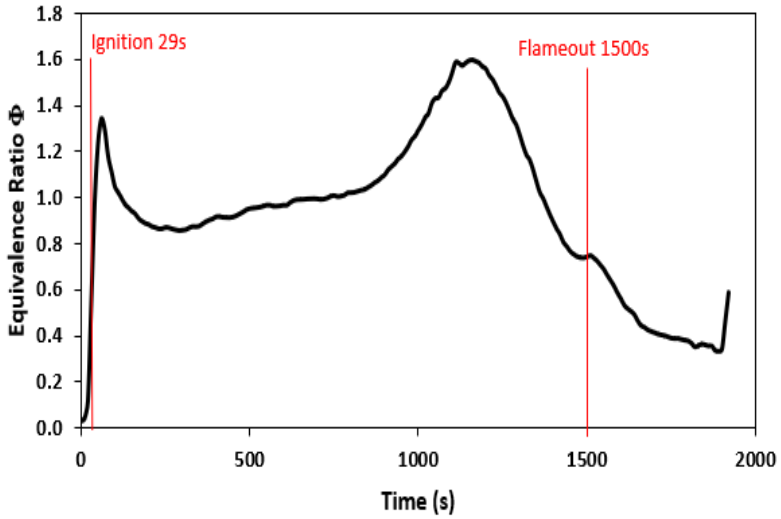

Fig. 9. Equivalence ratio by carbon balance of the raw primary gas composition

The equivalence ratio by carbon balance of the raw primary combustion hot exhaust gases is shown in Fig. 9 and this is much leaner at all times than in Fig. 8 by metered wood mass loss rate. However, although the measured A/F is based on carbon balance, the equivalence ratio calculation still assumes that the stoichiometric A/F is that of the original wood composition and not the material burning at a particular time. The oxygen readings in Fig. 7 indicate that the burning mixture in the 250 – 900 s was lean, as the combustion efficiency was high in this period. The CO results, discussed below, show two peaks at the times that Fig. 9 shows rich mixtures occurring, which is what would be expected. Thus, it is likely that Fig. 9 is a realistic equivalence ratio.

3.4 Gaseous Emissions Measurements

The toxic gases were measured from the raw sampling point of the cone calorimeter using the heated FTIR, with the gas sampling system described above. The main purpose of this work was the particle size analysis and sufficient toxic gas results are presented to identify the stages of the fire where gaseous toxic gases are high, so that the stages of high particle number emissions could be compared.

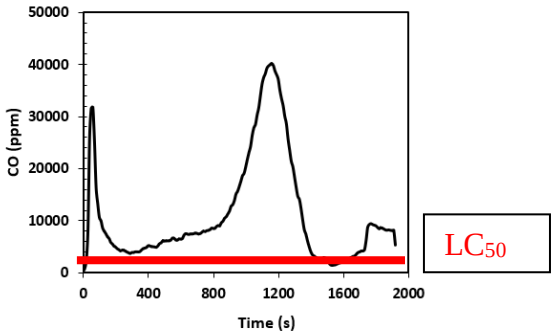

Fig. 10. CO concentration

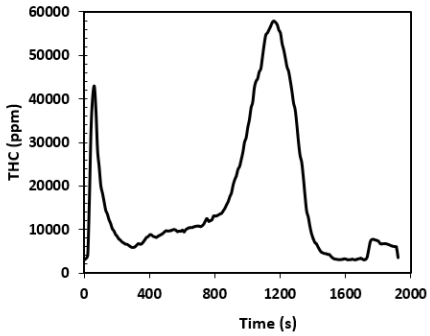

Fig. 11. Total Hydrocarbon Concentration (THC)

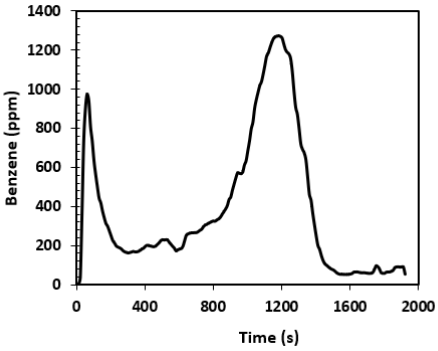

Fig. 12. Benzene Concentration

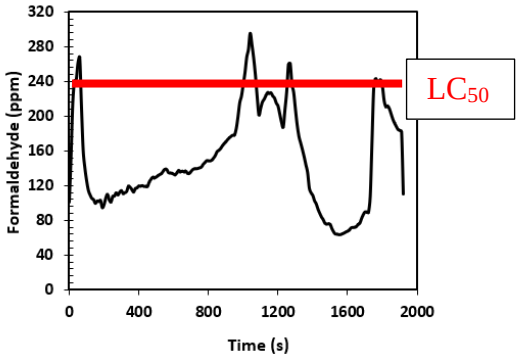

Fig.13. Formaldehyde Concentration

The FTIR results for CO, THC, benzene and formaldehyde are shown in Figs. 10-13 as a function of time. The LC_{50} toxic limits for CO and formaldehyde are marked. There is no LC_{50} limit for benzene, but the COSHH 15 min. limit for impairment of escape is 3 ppm and Fig. 8 shows concentrations over 100 times this level. Fig. 10 shows that there were two peaks in CO: in the initial flaming combustion period up to 200 s and from 800 – 1200 s, the first peak was 3 % and the second 4 %. Both peaks in CO occur at the same time the peaks in equivalence ratio in Fig. 9 and this would generate higher CO from equilibrium chemistry. In the same two-time periods Fig. 11 shows that there was an initial 4 % peak in THC with the second 6 % peak in THC at the same time as the second CO peak. These are very high levels of CO and unburned hydrocarbons with a very large energy content that is released in the second stage combustion external to the chimney. Each individual hydrocarbon also showed the same two peaks in emissions as illustrated by the results for benzene in Fig. 12, where the first flaming combustion peak was 1000 ppm and the second peak was 1300 ppm. Formaldehyde emissions are shown as a function of time in Fig. 13 and this shows three peaks, the first two aligned with those for THC and the third peak was at 1700-1900 s in the char combustion period.

The CO yield as a function of the metered equivalence ratio is shown in Fig. 14. This shows that the equivalence ratio alone is insufficient to determine the CO yield as at the start and end of the fire the CO emissions were different for the same equivalence ratio. This phenomenon has also been found by the authors in pine wood crib compartment fires, using the same pine material as in the present work [27]. In this case the fire ceiling temperature was the other variable for the same equivalence ratio. In the present work there was no measurement of the fire zone temperature, but it is likely that this was the other variable in the present work. Fig. 14 shows there was a high CO phase of the fire for lean combustion at the start and end of the fire. At the end of the fire the CO was from char combustion with lower burning rates and at the start of combustion the lean region was due to the start of volatilisation of the wood in the wood heating phase.

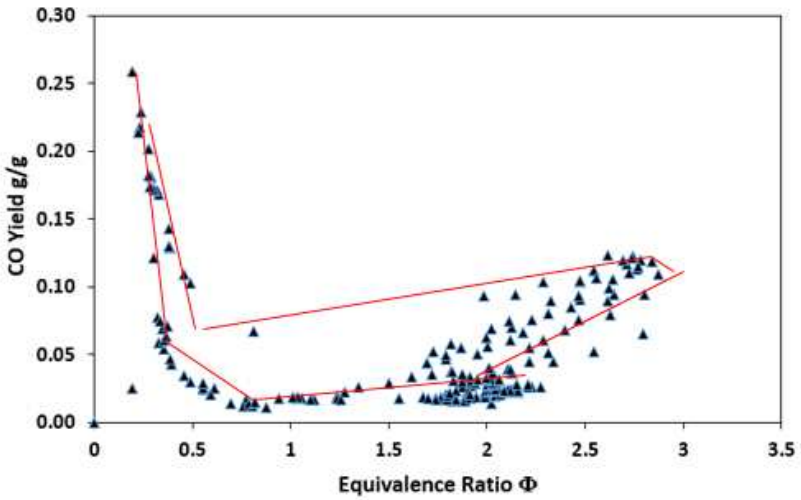

Fig. 14. CO yield (g/g) as a function of the fire equivalence ratio

3.5 Particle Size Number Distribution

Fig. 15 shows the particle number concentration and size distributions from the start of the test to the end of sampling. Fig. 16 shows some individual size distribution at defined times, which is easier to read the particle number. The initial particle size distribution during the ignition delay period showed only nano particles with a peak at 20 nm. These are likely to be liquid hydrocarbon aerosols and the high peak in THC in this period supports this. Once flaming combustion started there was a bimodal size distribution of nuclei particles centered on 20 nm and accumulation mode particles centered on 200 nm. The number-based size distribution was reasonably consistent from 100 to 1500 s, which is

the main flaming combustion period. There were differences in size distribution in the char burning phase of the fire, with a reduction in the number of accumulation mode particles.

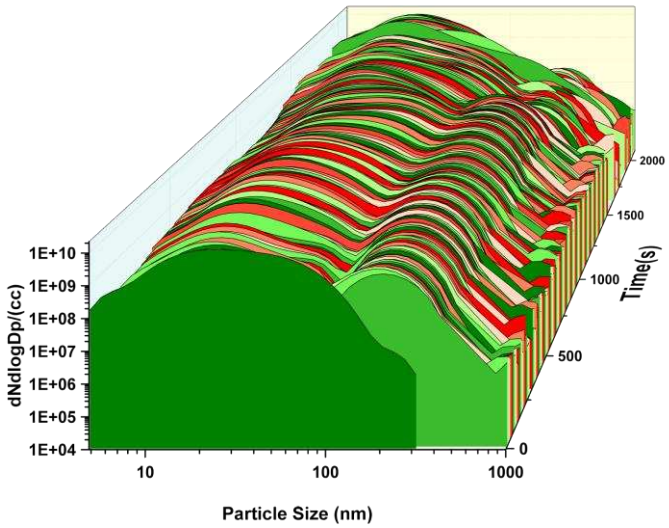

Fig. 15. Smoke particle number and size distribution

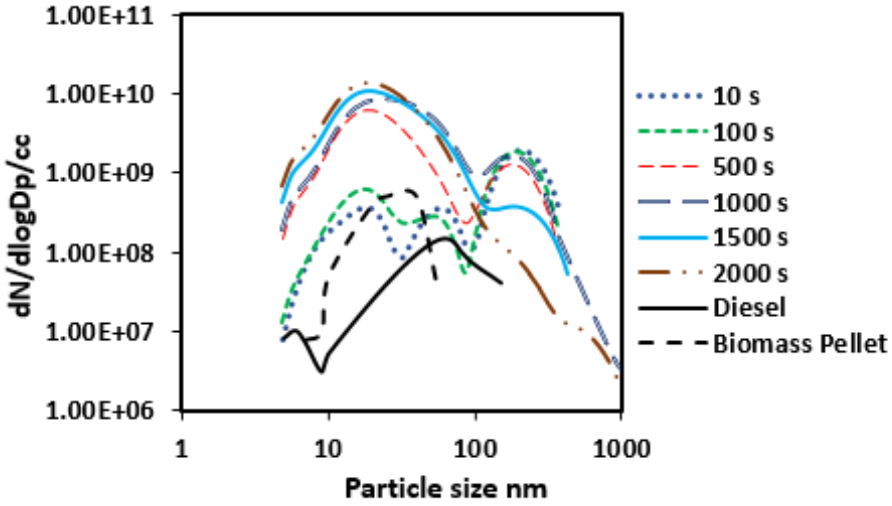

Fig. 16. Comparison of Particle number distribution with Diesel [31] and wood pellet boiler test [7]

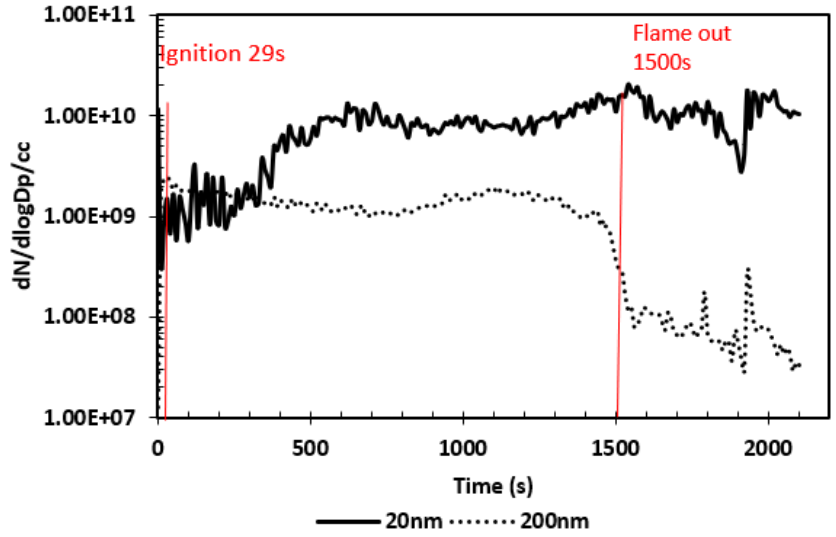

Fig. 17. 20nm and 200nm sizes particle number

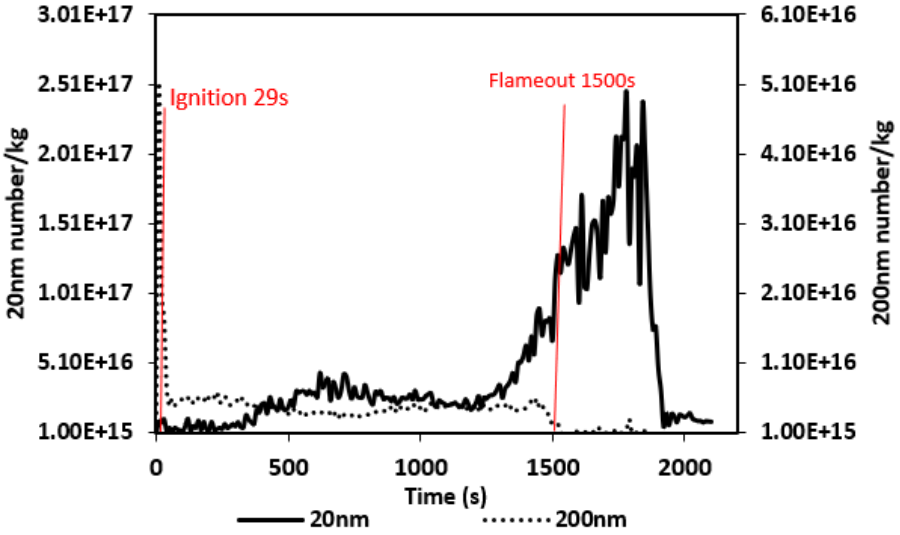

Fig. 18. Particle number per mass of fuel burnt for 20nm and 200nm particles as a function of time.

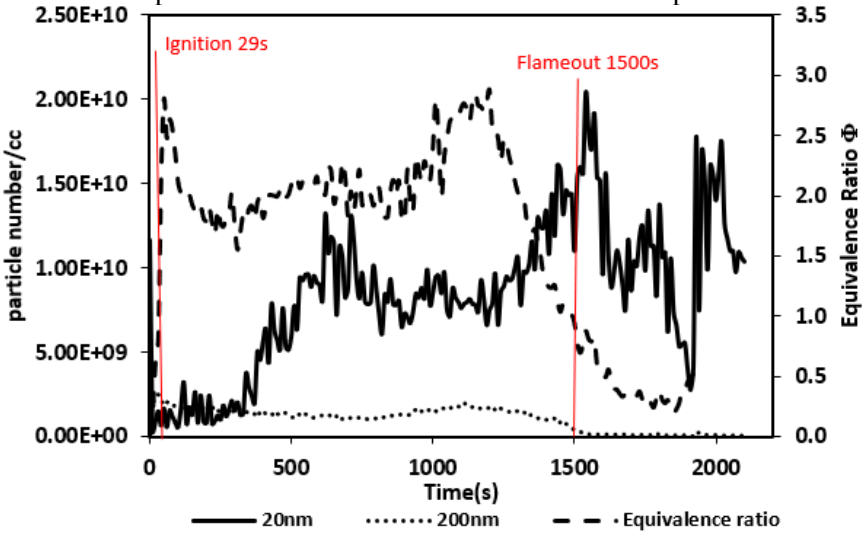

Fig. 19. Particle number per volume compared with the equivalence ratio variation with time.

There have been relatively few previous measurements of particle size distribution in fires and none to

our knowledge in simulated or real compartment fires. Hertzberg et al [15, 32] used the Dekati ELPI aerodynamic particle size analylser to measure the particle number from 40 to 10µm for a range of fire materials for the cone calorimeter. At 200 nm the particle number varied from 10^5 – 10^8 p/cm^3, with the highest value for an unspecified wood. In the present work for pine wood at 200 nm there were 10^9 p/cm^3 and the higher value is likely to be due to the simulation of a compartment fire using the modified cone calorimeter. Goo [33] has also used the ELPI aerodynamic size analyser for wood fires with the Purser steady state furnace method and reported particle number of 10^7 p/cm^3 at 200 nm, but the equivalence ratio of the tests were not given. These measurements are well below those in the present work. However, the Purser tube furnace method has a variable dilution ratio, which depends on the fire equivalence ratio that is simulated and varies between 5 and 25/1. If the measured particle number are corrected back to the concentration at the tube exit then they would increase by a factor of about ten and then be in better agreement with the present work. No measurements exist for particle number emissions from fires, to our knowledge, in the 5-40 nm size range, which are responsible for the greatest health risks as it is this size of particles that accumulate in the alveolar regions of the lungs and for the finest particles penetrate into the blood stream.

Fig.16 also compares the particle number distribution at different times during the test with tests from biomass pellets in a heater [7] for boilers and Euro 2 Diesel [31]. This shows that the present pine wood cone calorimeter compartment fire tests produced very high ultrafine particles compared to the diesel and the biomass pellets. The 20 nm size was about 100 times higher than that produced from the diesel or the biomass pellet. The accumulative mode was also at least a factor of 10 higher in number. This means that fine particles are produced in fires in much greater quantities than the more controlled combustion of diesel engines and biomass pellet heaters.

Fig. 17 shows, as a function of time, the 20 nm and 200 nm sizes particle number, as characteristic of the nuclei and accumulative mode particles. The 20 nm nuclei particle number increased from 10^9/cc to a peak at 10^{10}/cc for the first 700 s. There was then a reduction by 30 % from 700 – 1000 s and then an increase to 1.3 x 10^{10}/cc just before the flame out. High 20 nm particles continued to be produced in

the char burning phase, but there was a much-reduced accumulative mode particle number.

The 200 nm accumulation mode particles were produced at 1 x 10^9/cc throughout the flaming phase and then reduced to <1 x 10^8/cc in the smoldering phase of the combustion. Particles 30 nm – 100 nm had lower concentrations than the 20 nm particles. The small size found in the present work is of great concern as that is where the greatest health hazard occurs. Particle number concentrations were highest when the heat release was at its peak and gradually decreased after the flameout.

The toxic gas emissions showed a peak in the initial flaming combustion development at about 100 s and at 1000 – 1400 s. These were associated with peaks in the mean equivalence ratio of the fire and with peaks in the HRR at about 100 and 1300 s in Fig. 8. The second peak in the toxic gas emissions did coincide with the peak in 20 nm particle number, but there was no initial peak in 20 nm particles with flaming combustion. It will be shown below that the mass of accumulative mode particles has the best correlation with the toxic gas peak emission times.

Fig. 18 shows the particle number for 20 nm and 200 nm particles as a function of the mass of wood burnt. This shows that for both particle sizes the particle number has a fairly constant relationship with the fuel mass burn rate. In the present work the air mass flow is constant so that the variation of equivalence ratio and mass burn rate in Fig. 8 is responsible for the trends in particle number. Only in the smoldering combustion phase of the fire were the trends in particle number different for 20 and 200 nm, with an increase in yield of 20 nm particles and a decrease with 200 nm particles.

3.6 Particle Mass Distribution

The equivalent mass distributions are shown in Figs. 20 - 22. Figs. 20 and 21 show that there was less mass in the ultrafine particle region as compared to particles >100 nm, as expected, due to the particle volume and mass scaling with the cube of the particle diameter. Fig. 22 shows that the 20 nm particle size had a mass of about 0.1 g/m^3 and that the 200 nm mode had a mass of 10 g/m^3 during the flaming phase of the combustion. It is also clear in Fig. 21 that there is more particle mass above the 1000 nm

upper measurement range of the Cambustion DMS500. In air quality legislation for particulate emissions the European 24 hour limit for $PM_{2.5}$ is 50 µg/m^3 and the annual limit is 40 µg/m^3. The 24 hour limit is a total particulate loading, for an average human breathing 10 m^3 of air per day, of 0.5 mg/day. Exposure to the present pine wood fires would give a lung loading of 1 g per day of 20 nm particles and 100 g per day of 200 nm particles. For 20 nm particles this is 200 times the mass loading per day of PM_{10} and for 200 nm particles it is 2000 times the fine particulate mass loading of a poor air quality day in terms of PM_{10} air quality. This represents a major health risk to people who breathe wood based particulates in fires. The situation will be worse for hydrocarbon based building products, as smoke yields are known to be about six times those for wood [34].

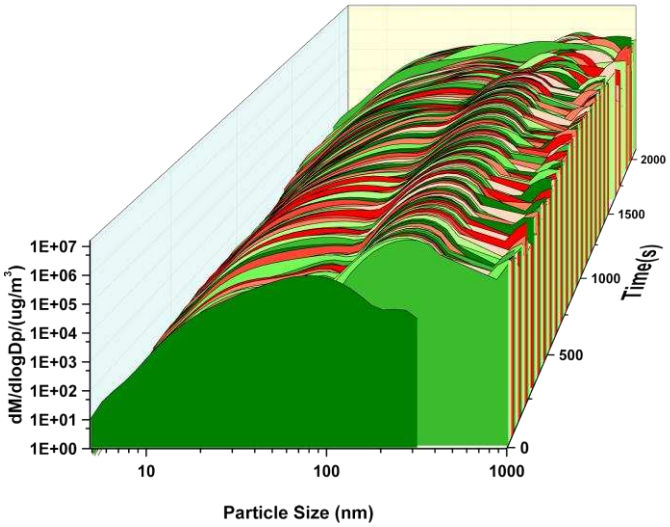

Fig. 20. Particle mass size distribution µg/m^3

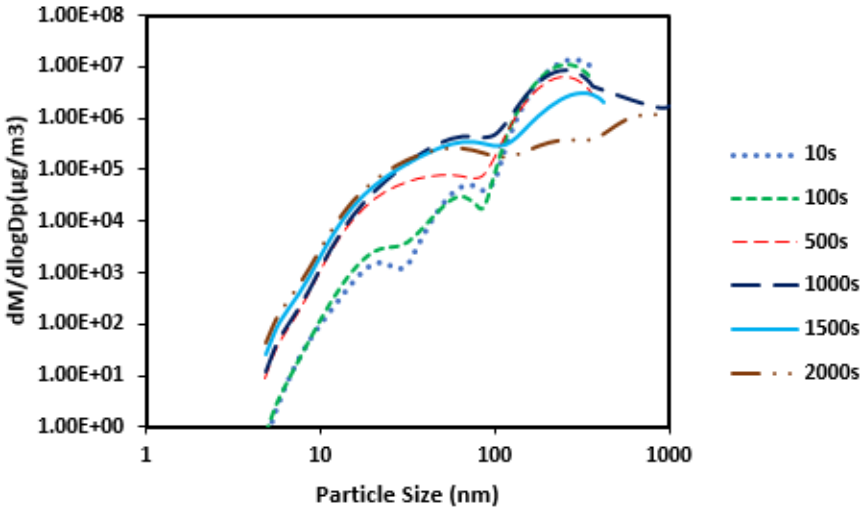

Fig. 21. Particle number and size distributions at different burning time

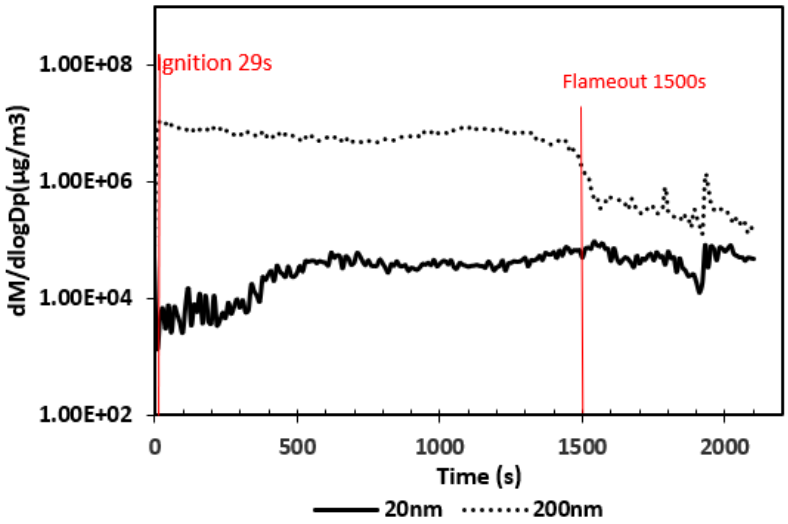

Fig. 22. 20nm and 200nm sizes particle mass

3.7 Smoke Obscuration and Particle Mass Comparison

The cone calorimeter measures the smoke optical obscuration in the diluted gases from the simulated compartment fire, using visible light with a typical wavelength of 0.55 µm. The specfic extinction coefficient is about 2 m^2/g at 0.55 µm wavelength for 1 µm particles size and 7 m^2/g at 0.2 µm, for particles of carbon with 50 % by weight of hydrocarbons [35]. Fig. 23 shows that for most of the present work the mass of particulates per volume of gas flow in the chimney for 0.2 µm particles had similar trends to the smokemeter. However, from a health hazard point of view it is the number of particles <50 nm that matters and particles of this size have negligible obscuration or light scattering [35] and hence do not correlate with the smoke number, as shown in Fig. 24. This means that the ranking of toxic products of materials in fires, using the smokemeter reading on the cone calorimeter, is not valid for the toxiciy of fine particles.

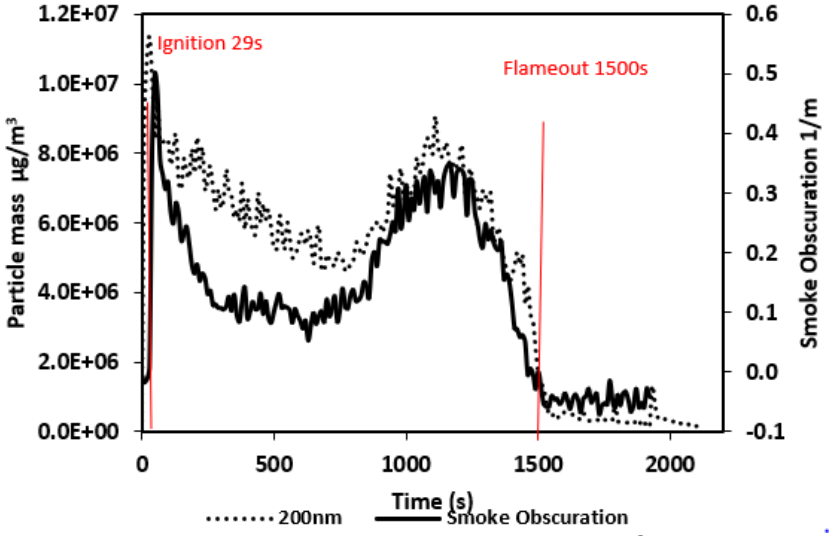

Fig. 23. Smoke obscuration measurements compared with the mass / m^3 of the 200nm particles.

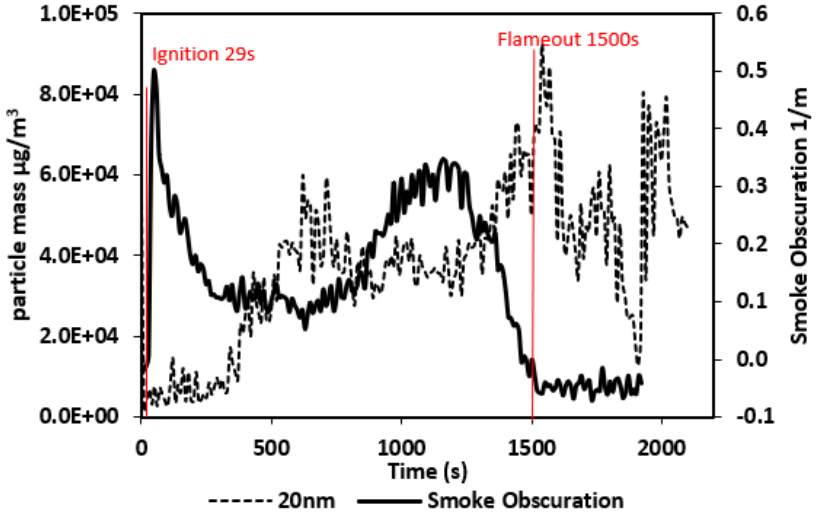

Fig. 24. Smoke obscuration measurements compared with the mass of 20nm particles

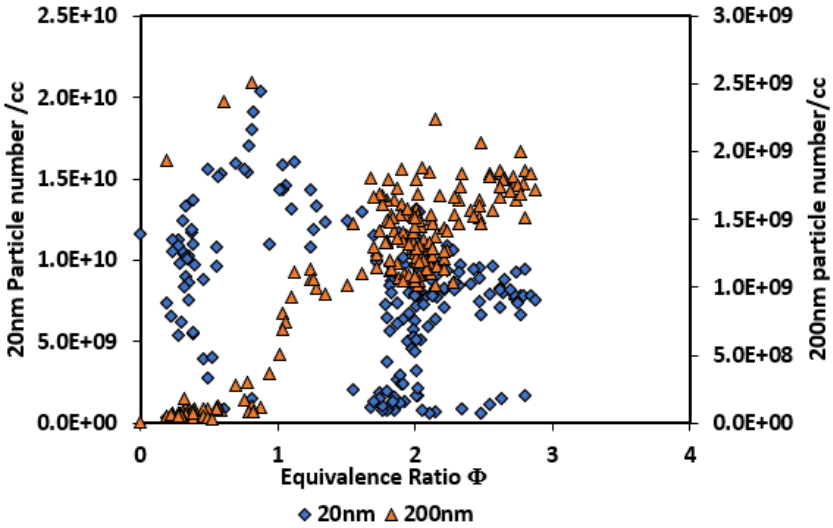

Fig. 25. Particle number per volume as a function of the metered equivalence ratio for 20nm and 200 nm particle size

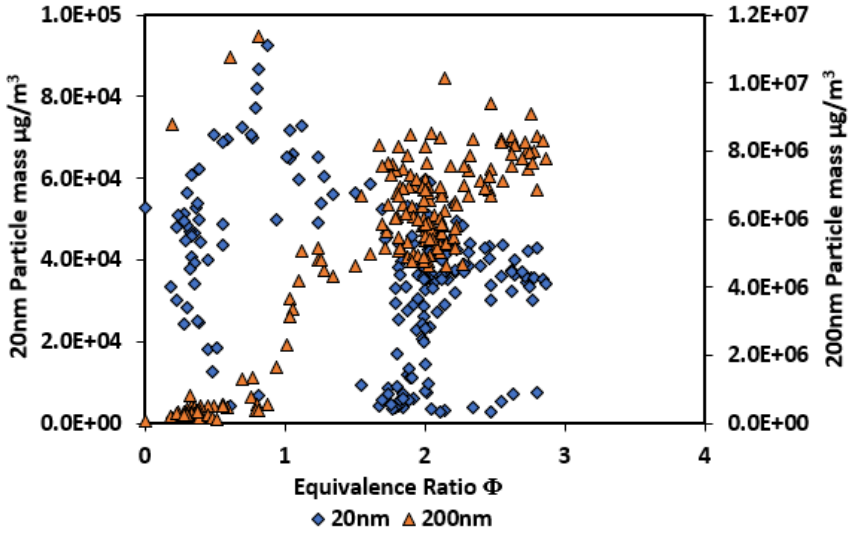

Fig. 26. Particle mass per volume as a function of fire equivalence ratio for 20nm and 200nm particles.

CONCLUSIONS

The real - time particle size, number and mass distribution from pine wood combustion was obtained showing a bimodal distribution representing a nucleation mode and an agglomeration/accumulation mode. The particle size distribution on a number basis showed a peak of 20 nm in the nano particle size range and a peak of 200 nm in the agglomeration range. Ultra – fine particles generated in wood combustion was higher than those generated by diesel engines or biomass pellet combustion. These nano particles (20 nm) will penetrate the lungs in the event of fire leading to impairment of escape and eventually death due to the effects that fine particles have on the lungs thereby making it a major toxic hazard in fires. There's need for a review of the legislation on fire tests to include particle production tests considering the threat it poses. The modified cone calorimeter proved to be a good technique for realistic determination of particle size distributions in fires when used with the FTIR and the DMS 500

ACKNOWLEDGMENTS

Bintu Grema Mustafa would like to thank the Petroleum Technology Development Fund, Nigeria and the University of Maiduguri for sponsoring her PhD. The Ministry of Higher Education and the Universiti Teknologi Malaysia are acknowledged for sponsoring M.H. Mat Kiah's PhD. The University of Engineering & Technology, Lahore, Pakistan is thanked for a Faculty Development Programme (FDP) PhD Scholarship to A. Irshad. The DMS 500 and FTIR were provided by the UK EPSRC as part of the LANTERN and RETEMM research programmes.

REFERENCES

[1] A. Violi, Effects of Combustion-Generated Nanoparticles on Cellular Membranes, Combustion Science and Technology, 188 (2016) 769-775.
[2] C.A. Pope, R.L. Verrier, E.G. Lovett, A.C. Larson, M.E. Raizenne, R.E. Kanner, J. Schwartz, G.M. Villegas, D.R. Gold, D.W. Dockery, Heart rate variability associated with particulate air pollution, American Heart Journal, 138 (1999) 890-899.
[3] J.S. Lighty, J.M. Veranth, A.F. Sarofim, Combustion aerosols: factors governing their size and composition and implications to human health, Journal of the Air & Waste Management Association (1995), 50 (2000) 1565-1618.
[4] A. Seaton, D. Godden, W. MacNee, K. Donaldson, Particulate air pollution and acute health effects, The Lancet, 345 (1995) 176-178.
[5] A. Peters, H.E. Wichmann, T. Tuch, J. Heinrich, J. Heyder, Respiratory effects are associated with the number of ultrafine particles, American journal of respiratory and critical care medicine, 155 (1997) 1376-1383.
[6] A. Kocbach Bølling, J. Pagels, K.E. Yttri, L. Barregard, G. Sallsten, P.E. Schwarze, C. Boman, Health effects of residential wood smoke particles: the importance of combustion conditions and physicochemical particle properties, Particle and Fibre Toxicology, 6 (2009) 29.
[7] M.A. Altaher, G.E. Andrews, B.M. Gibbs, S.A. Hadavi, H. Li, E. Jones, M. Mercer, Comparison of Gaseous and Particulate Emissions from Wood Pellet and Oil Fired Combustion for the same Heat Input, in: The 10th European Conference on Industrial Furnaces and Boilers (INFUB-10), Porto, Portugal, 2015.
[8] L.S. Johansson, B. Leckner, L. Gustavsson, D. Cooper, C. Tullin, A. Potter, Emission characteristics of modern and old-type residential boilers fired with wood logs and wood pellets, Atmospheric Environment, 38 (2004) 4183-4195.
[9] G.E. Andrews, J. Ledger, H.N. Phylaktou, The Gravimetric Determination of Soot Yields in Enclosed Pool Fires, in: 3rd International Colloquia on Explosions in Reactive Systems, Windermere, 2000.
[10] G. Migliavacca, S. Marengo, F. Hugony, C. Morreale, A. Maggioni, S. Bertagna, Ultrafine Particles from Biomass Combustion in Small Scale Heating Systems, in: 18th European Biomass Conference and Exhibitio, Lyon, France, 2010, pp. 1321-1326.
[11] T. Nussbaumer, A. Lauber, Formation Mechanisms and Physical Properties of Particles from Wood Combustion for Design and Operation of Electrostatic Precipitators, in: 18th European Biomass Conference and Exhibition, Lyon, France, 2010, pp. 1219 - 1227.
[12] A. Bologa, H.-R. Paur, H. Seifert, K. Woletz, T. Ulbricht, Fine Particle Generation, Evolution and Control By Small Scale Biomass Combustion Devices, in: 18th European Biomass Conference and Exhibition, Lyon, France, 2010, pp. 1208 - 1218.
[13] J.-B. Michel, C. Mahmed, J. Ropp, J. Richard, M.A. Sattler, M. Schmid, Combustion Evaluation of Torrefied Wood Pellets on a 50 KWth Boiler, in: 18th European Biomass Conference and Exhibition, Lyon, France, 2010, pp. 1534 - 1540.
[14] P. Blomqvist, T. Hertzberg, H. Tuovinen, K. Arrhenius, L. Rosell, Detailed determination of smoke gas contents using a small-scale controlled equivalence ratio tube furnace method, Fire and Materials, 31 (2007) 495-521.
[15] T. Hertzberg, P. Blomqvist, Particles from fires—a screening of common materials found in buildings, Fire and Materials, 27 (2003) 295-314.
[16] B.I. 5660-1:2015, BS ISO 5660-1:2015: Reaction-to-fire tests. Heat release, smoke production and mass loss rate. Heat release rate (cone calorimeter method) and smoke production rate (dynamic measurement), in, British Standards Institute, 2015.
[17] C. Huggett, Estimation of rate of heat release by means of oxygen consumption measurements, Fire and Materials, 4 (1980) 61-65.
[18] K.W. Flecknoe-Brown, K. Livkiss, P. Van Hees, Experimental and Numerical Investigation on Fire Behaviour of Foam/Fabric Composites, in: 15th International Conference, Fire and Materials, Interscience Communications, San Francisco, USA, 2017, pp. 240-253.
[19] A.A. Alarifi, H.N. Phylaktou, G.E. Andrews, Heated Raw Gas Sampling with Heated FTIR Analysis of Toxic Effluents from Small and Large Scale Fire Tests, in: 10th Asia-Oceania

667 Symposium on Fire Science and Technology, IAFSS, Tsukuba, Japan, 2015.
668 [20] E.M. Fitzpatrick, A.B. Ross, J. Bates, G. Andrews, J.M. Jones, H. Phylaktou, M. Pourkashanian,
669 A. Williams, Emission of Oxygenated Species from the Combustion of Pine Wood and its Relation to
670 Soot Formation, Process Safety and Environmental Protection, 85 (2007) 430-440.
671 [21] D.B. Kittelson, W.F. Watts, J.P. Johnson, On-road and laboratory evaluation of combustion
672 aerosols—Part1: Summary of diesel engine results, Journal of Aerosol Science, 37 (2006) 913-930.
673 [22] I. Abdul-Khalek, D. Kittelson, F. Brear, The Influence of Dilution Conditions on Diesel Exhaust
674 Particle Size Distribution Measurements, in, SAE International, 1999.
675 [23] Cambustion, DMS500 Fast Particulate Spectrometer with Heated Sample Line High Ratio Diluter
676 User Manual, in, Cambridge, 2011.
677 [24] G.E. Andrews, B. Daham, M.D. Mmolawa, S. Boulter, J. Mitchell, G. Burrel, J. Ledger, W.
678 Gunamusa, R.A. Boreham, H.N. Phylaktou, FTIR Investigations of Toxic Gases in Air Starved
679 Enclosed Fires, in: D.a.L.B.Y. Gottuk (Ed.) 8th International Symposium on Fire Safety Science,
680 International Asssociation for Fire Safety Science, Beijing, 2006.
681 [25] G.E. Andrews, H. Li, A. Hunt, D. Hughes, S. Bond, P. Tucker, S. Akram, H.N. Phylaktou, Toxic
682 Gases in Simulated Aircraft Interior Fires using FTIR Analysis, in: 5th Internation Conference on Fire
683 and Explosion Hazards, University of Edinburgh, 2007, pp. 846-855.
684 [26] O. Aljumaiah, S. Alshammari, G. Burrel, M. Cox, G.E. Andrews, H.N. Phylaktou, Toxic
685 Emissions from Folded Cotton Towels in a Low Ventilation Compartment, in: 6th International
686 Conference on Fire and Explosion Hazards, University of Leeds, UK, 2010, pp. 792-803.
687 [27] O. Aljumaiah, G.E. Andrews, H.N. Phylaktou, B.G. Mustafa, H. Al-Qattan, V. Shah, Air Starved
688 Compartment Wood Crib Fire Heat Release and Toxic Gas Yields, in: Fire Safety Science -
689 Proceedings of the Tenth International Symposium, International Association for Fire Safety Science,
690 2011, pp. 1263-1276.
691 [28] A.A. Alarifi, J. Dave, H.N. Phylaktou, O.A. Aljumaiah, G.E. Andrews, Effects of fire-fighting on
692 a fully developed compartment fire: Temperatures and emissions, Fire Safety Journal, 68 (2014) 71.
693 [29] G.E. Andrews, A.G. Clarke, N.Y. Rojas, T. Sale, D. Gregory, Diesel Particle Size Distribution:
694 The Conversion Of Particle Number Size Distribution To Mass Distribution, in, SAE International,
695 2001.
696 [30] M. Janssens, Calorimetry, in: P.J. DiNenno (Ed.) SFPE Handbook of Fire Protection Engineering,
697 National Fire Protection Association, Quincy, MA, 2002, pp. 3-38.
698 [31] H. Li, A. Lea-Langton, G.E. Andrews, M. Thompson, C. Musungo, Comparison of Exhaust
699 Emissions and Particulate Size Distribution for Diesel, Biodiesel and Cooking Oil from a Heavy Duty
700 DI Diesel Engine, in, SAE International, 2008.
701 [32] T. Hertzberg, P. Blomqvist, M. Dalene, G. Skarping, Particles and Isocynates from fires, in:
702 S.S.N.T.a.R. Institute (Ed.) Brandforsk profect 324-021, SP Swedish National Testing and Research
703 Institute, Boras, Sweden, 2003.
704 [33] J. Goo, Study on the real-time size distribution of smoke particles for each fire stage by using a
705 steady-state tube furnace method, Fire Safety Journal, 78 (2015) 96-101.
706 [34] A. Tewerson, Generation of Heat and Chemical Compounds in Fires, in: P.J. DiNenno (Ed.)
707 SFPE handbook of fire protection engineering, National Fire Protection Association, Bethesda,
708 Md;Quincy, Mass;, 2002, pp. 3/83-83/161.
709 [35] D.M. Roessler, F.R. Faxvog, R. Stevenson, G.W. Smith, Optical Properties and Morphology of
710 Particulate Carbon: Variation with Air/Fuel Ratio, in: D.C. Siegla, G.W. Smith (Eds.) Particulate
711 Carbon: Formation During Combustion, Springer US, Boston, MA, 1981, pp. 57-89.
712